Electronic Supplementary Material (ESI) for Nanoscale.
This journal is © The Royal Society of Chemistry 2019
Please do not adjust margins

Nanoscale

ESI

Electrical and Geometrical Tuning of MoS2 Field Effect Transistors via Direct Nanopatterning

Received 00th January 20xx,
Accepted 00th January 20xx

DOI: 10.1039/x0xx00000x

www.rsc.org/

Fernando. J. Urbanos,[a] A. Black,[b] Ramón Bernardo-Gavito,[c] A. L. Vázquez de Parga,[a,d] Rodolfo Miranda,[a,d] and D. Granados *[a]

a. IMDEA NanoScience, C/Faraday, 9, 28049, Madrid, Spain.

b. Institute for Physical Chemistry, University of Hamburg, Grindelallee, 117, 20146, Hamburg, Germany.

c. Physics Department, Lancaster University, LA14YB, Lancasrer, United Kingdom.

d. Dep. Física de la Materia Condensada and IFIMAC, Universidad Autónoma de Madrid, Cantoblanco, 28049,Madid, Spain

* Contact email: daniel.granados@imdea.org

Different geometries can be achieved with PFEBIE patterning. Fig. S1 shows two examples of those structures. Fig. S1a represents a zig zag structure, where the channel's width is 100 nm. Fig. S1b shows a more complex geometry. In this case a 140 nm central quantum dot was formed within two MoS_2 contacts.

It is well known that the exfoliation method produces flakes with variation in thickness, size, number of layers, etc., but PFEBIE is a capable technique to minimize this apparent problem. Fig. S1c and S1d show how PFEBIE can be used to modify the geometry of a flake that has different thicknesses. Fig. S1c shows that the device has three different regions, each with a different layer number. Due to this problem, the electric behaviour will be difficult to understand since the bandgap will have different energies and band alignment. For that reason, PFEBIE was used to alter the geometry of this device. Fig. S1d shows that after the patterning the device has only one region with a uniform layer thickness, simplifying the electronic behaviour. We think that PFEBIE is demonstrated to be a technique that can solve an evident problem of exfoliation, avoiding intermediated fabrication steps.

Please do not adjust margins

Please do not adjust margins

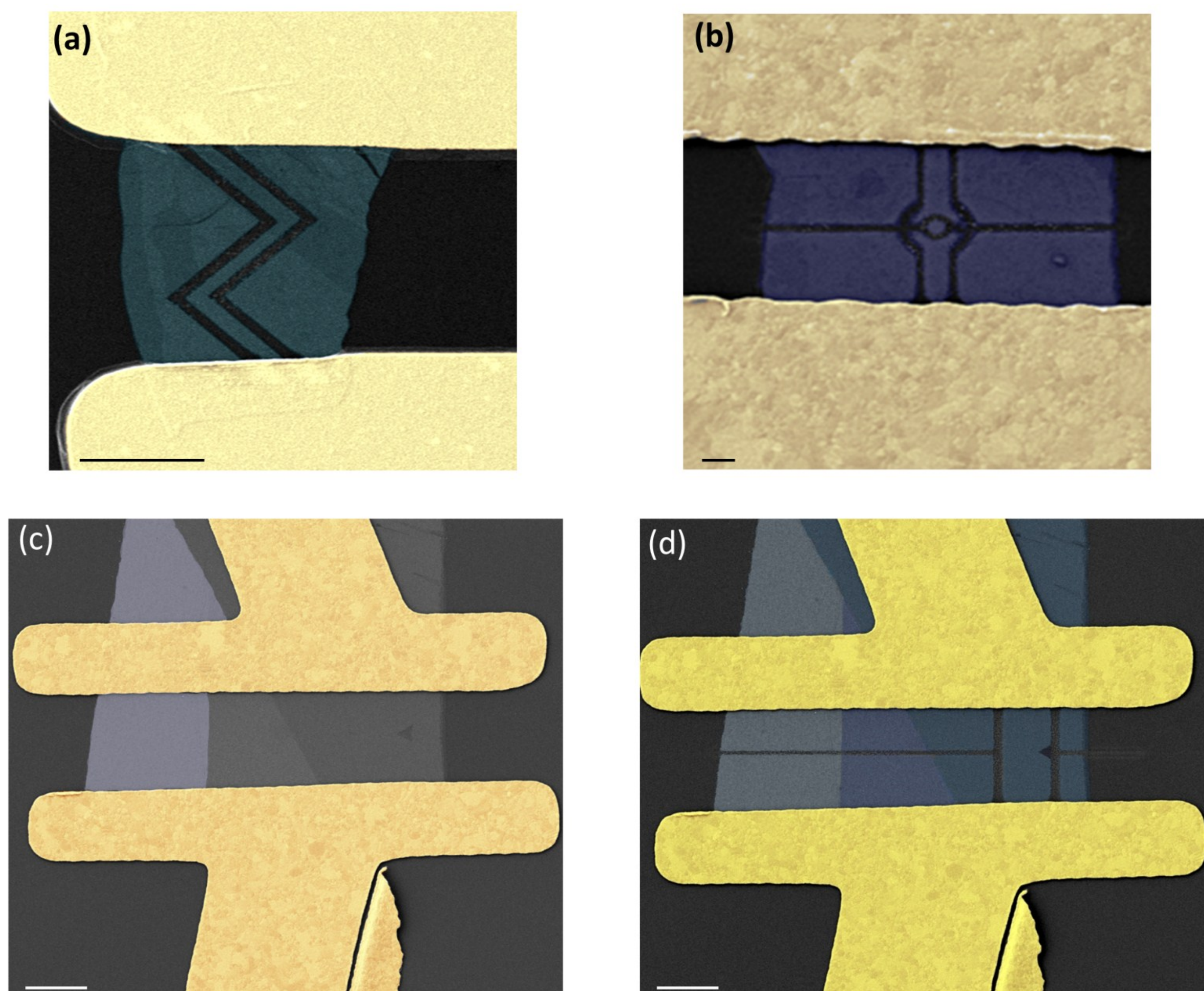

Fig.S1. False-colour SEM images of different geometries made with PFEBIE. (a) Zig zag structure with IMDEA Nanociencia logo. Scale bar is 2 µm. (b) MoS_2 quantum dot structure. Scale bar is 200 nm**. (c)** and **(d)** Another example of a tailored device. **(c)** Original device presenting three regions with different thicknesses. **(d)** Same device after PFEBIE. The device has now only one thickness. Scale bars in (c) and (d) are 2 µm.

This journal is © The Royal Society of Chemistry 20xx

Please do not adjust margins

Please do not adjust margins

The composition of the device could change between before and after steps due to the etching mechanism. For that reason, EDX measurements were performed in an exfoliated flake before and after PFEBIE. Due to the resolution of our equipment, a simple structure was fabricated to observe what the composition is in between etched areas, as Fig. S2b and S2c show. Fig. S2a shows the spectrum before (blue) and after (red) the patterning. Normalization was made taking into account the silicon peak, which is the element that supposedly does not vary between steps. The characteristic transitions of Si, Mo and S (at 1.739 KeV, 2.293 KeV and 2.307 KeV respectively) are within error exactly the same after the patterning with no signatures of additional fluorinated compounds or by-product materials. The inset of Fig. S2a shows a very small variation in the intensities between before and after steps. This variation could be attributed to changes in the total amount of MoS2 material, due to the etching process, rather than in its chemical composition. It is important to mention that there is a variation in the carbon peak. It increases due to carbon deposition when performing SEM characterization. EDX maps shown from Fig. S2d to S2j reveal that there was not a change in the composition of the flake. The characteristic transitions of Si (Fig. S2d and S2g), S (Fig. S2e and S2h) and Mo (Fig S2f and S2i) are the same between before and after steps. Fig. S2j shows that after the patterning there was not fluorine signal, indicating that fluorinated compounds or reaction by-products do not redeposit during the etching process.

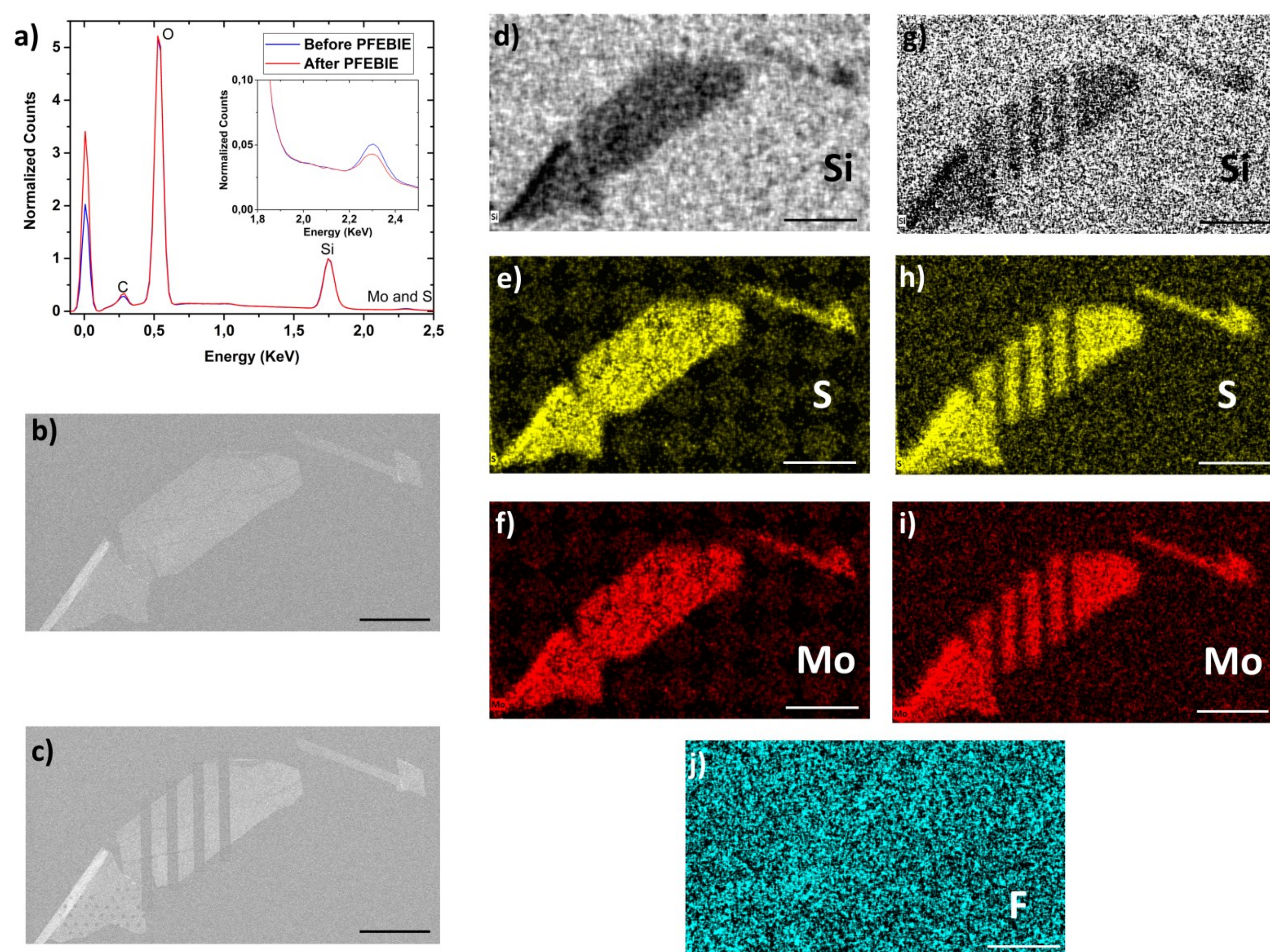

Fig.S2. EDX study of an exfoliated flake. a) EDX spectra of the flake before (blue) and after (red) the patterning. The inset shows a zoom of the Mo and S transitions at 2.293 and 2.307 KeV respectively b) SEM image of the initial flake. c) SEM image of the patterned flake. d) Kα transition of Si before the patterning. e) Kα transition of S before the patterning. f) Lα transition of Mo before the patterning. g) Kα transition of Si after the patterning. h) Kα transition of S after the patterning. i) Lα transition of Mo after the patterning. j) Fluorine Kα transition after the patterning showing that there is no presence of fluorinated compounds or reaction by-products. Scale bars are 4 µm

Please do not adjust margins

Please do not adjust margins

Additional BSE images before and after the patterning were taken. Fig. S3 shows an BSE image of the device before and after the patterning. The contrast remains similar between the before and after step, indicating that the composition did not change in an apreciable manner.

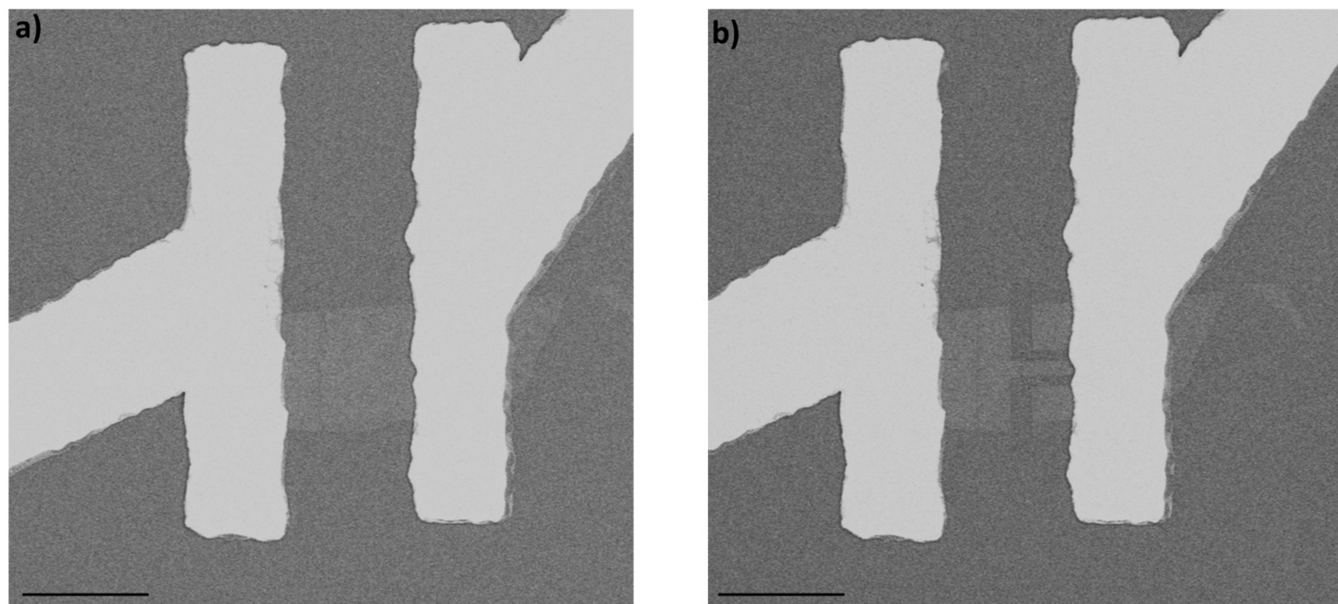

Fig.S3. BSE images of a device. a) BSE image before the patterning. b) BSE image after the patterning. The contrast remains equal between steps, indicating that there was not change in the composition. Scale bars are 3 μm

This journal is © The Royal Society of Chemistry 20xx

Please do not adjust margins

Please do not adjust margins

The power of PFEBIE resides on controlling the width and geometry of the conduction channel. For that reason, it is important to show that the method is reproducible. Consequently, Fig. S4 shows SEM images of the devices shown in Fig. 2b. In all cases, the channel width was nominally set to 250 nm. Most of the devices have a cross-bar shape to avoid electrical conductivity. In the rest of the cases, the flake was properly etched to ensure conduction through the wired channel.

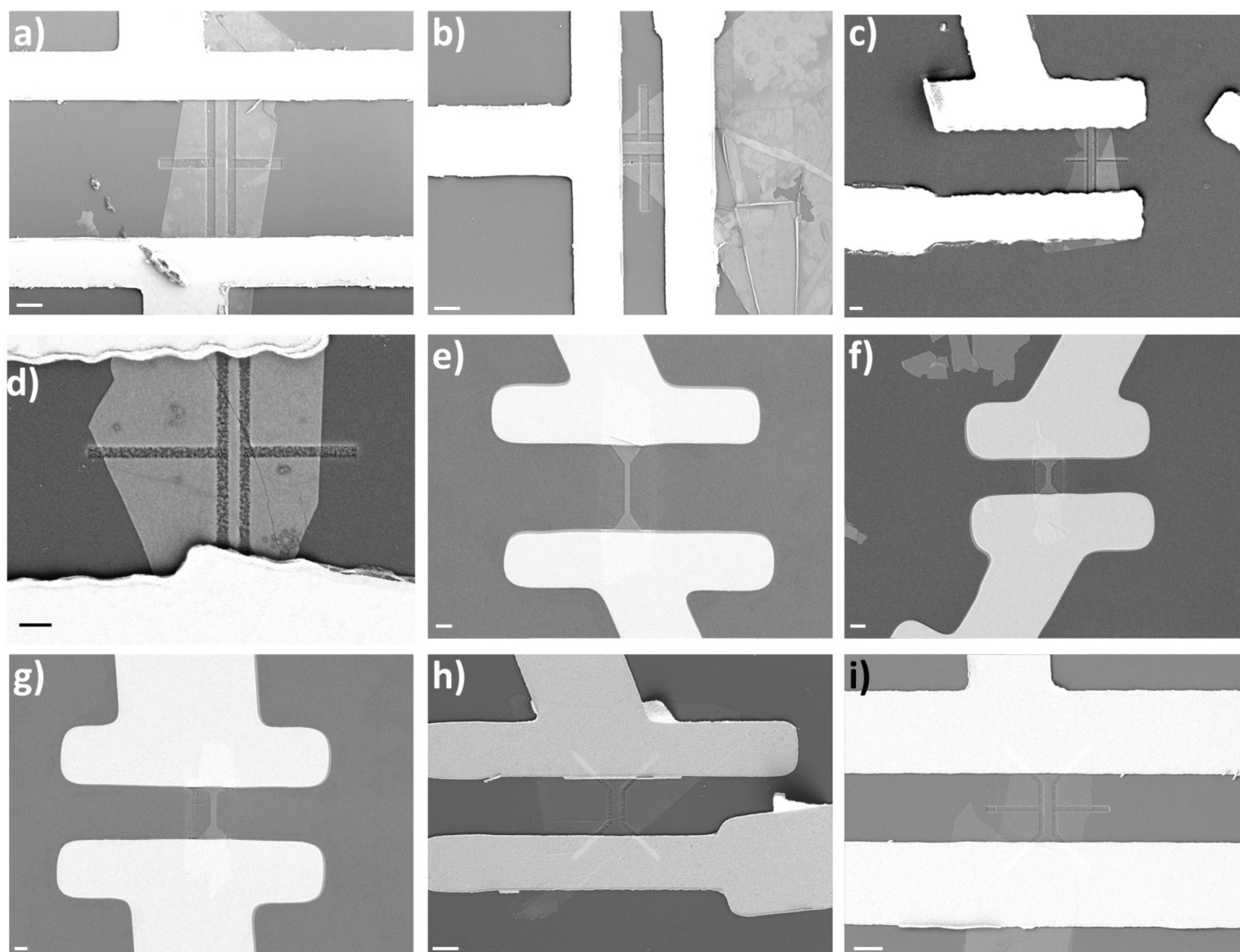

Fig.S4. SEM images of the devices shown in Fig. 2b.**a)** Device 2 of Fig. 2b. **b)** Device 6 of Fig. 2b. **c)** Device 3 of Fig. 2b. **d)** Device 10 of Fig. 2b. **e)** Device 1 of Fig. 2b. **f)** Device 4 of Fig. 2b. **g)** Device 8 of Fig. 2b. **h)** Device 9 of Fig. 2b. **i)** Device 5 of Fig. 2b. Scale bars are 500 nm.

Please do not adjust margins

Please do not adjust margins

The electric behavior was studied in more samples. Fig. S5 shows the drain current as a function of the gate voltage. It shows a change in the threshold voltage, from -60 V to -30 V (calculated with the approximation in the linear region method).[1] In this case we observe a change from negative to less negative values of the threshold voltage, e.g. is a change from N^{++} to N^{+} doping. The gate voltage measuring range is limited, making impossible to completely measure the tailored devices. For that reason, it is difficult to compare the original and the tailored device. The characteristic states (saturation, linear region, off state and threshold voltage) appear in different gate voltages.

The mobility can be extracted from the following formula:

$$\mu = \frac{L}{W \cdot C_{ox} \cdot V_d} \cdot \frac{dI_d}{dV_g}$$

Where L and W are length and the width of the device respectively. V_d is the applied drain voltage. C_{ox} is the oxide capacitance, which depends on the oxide thickness, and the vacuum and relative permittivity (d, ε_0, ε_r respectively) and can be expressed as $\frac{\varepsilon_0 \cdot \varepsilon_r}{d}$. The oxide thickness is 285 nm and ε_0 is 3.9 for MoS_2 The transconductance is expressed as $\frac{dI_d}{dV_g}$.

The mobility of the original device is 18.2 $cm^2\ V^{-1}\ s^{-1}$. After PFEBIE, this saturation region is not observed. Despite of this, the mobility can be approximately calculated in the expected linear region, resulting in 6.4 $x10^{-3}$ $cm^2\ V^{-1}\ s^{-1}$. It was dramatically reduced, maybe due to the creation of defects when the etching was performed.[2-4]

The intrinsic device shows a ON/OFF ratio of 10^5. The ON/OFF ratio after PFEBIE is unknown because the saturation region is above the gate voltage measuring range.

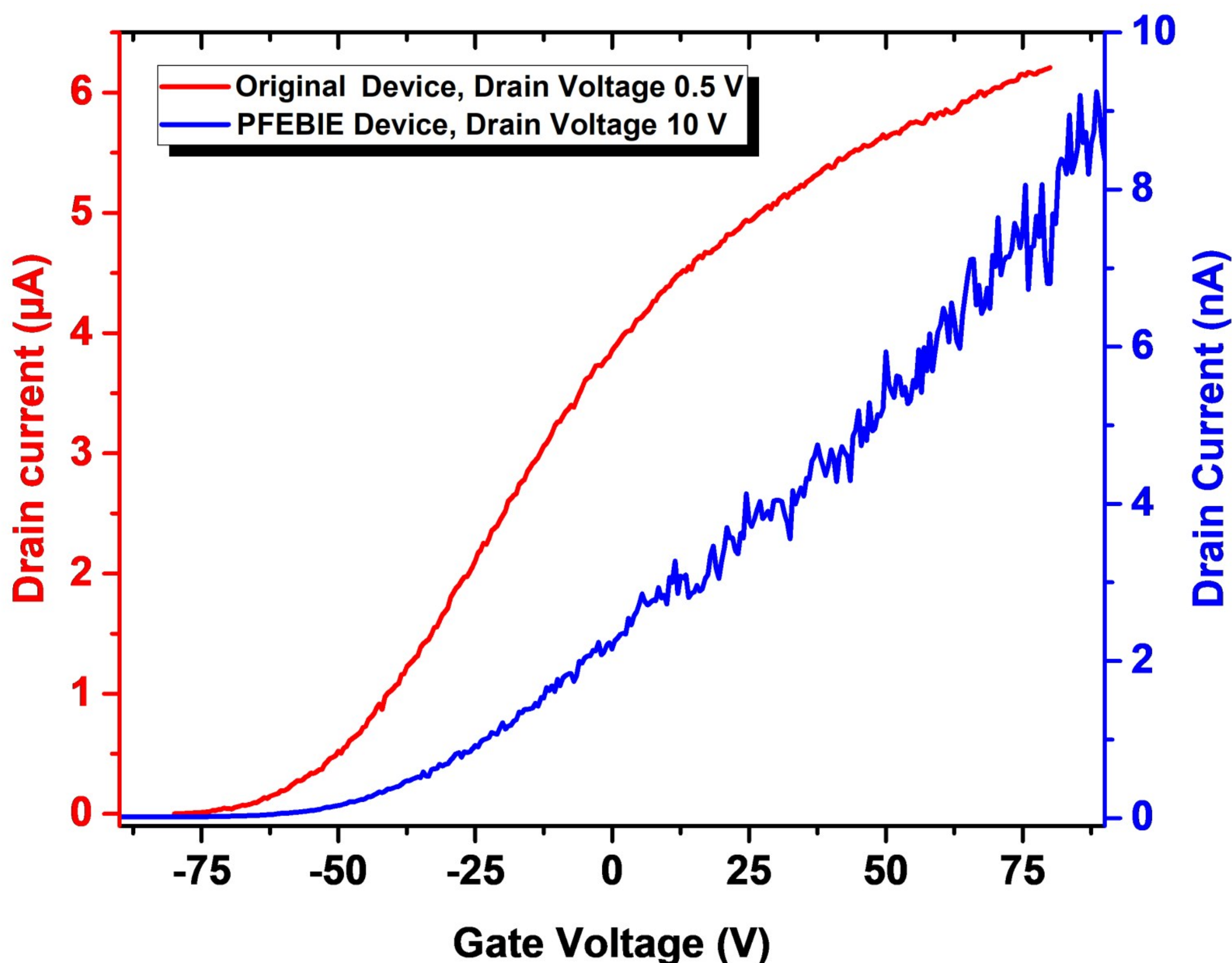

 This journal is © The Royal Society of Chemistry 20xx

Please do not adjust margins

Please do not adjust margins

Fig.S5. Room temperature Voltage-Current characteristics of a FET device before (red) and after (blue) PFEBIE. Threshold voltage changes from -70 V to -30 V.

Fig. S6 represents the A_{1g} full width at half maximum (FWHM) map. A change from 7.5 cm^{-1} to 9 cm^{-1} is observed, in the same direction we observed the E^1_{2g} peak. In average, an increase of 1.5 cm-1 is observed. Irradiation may cause a partial removal of sulfur, creating Raman peak shifts as the observed in our experiments.[5]

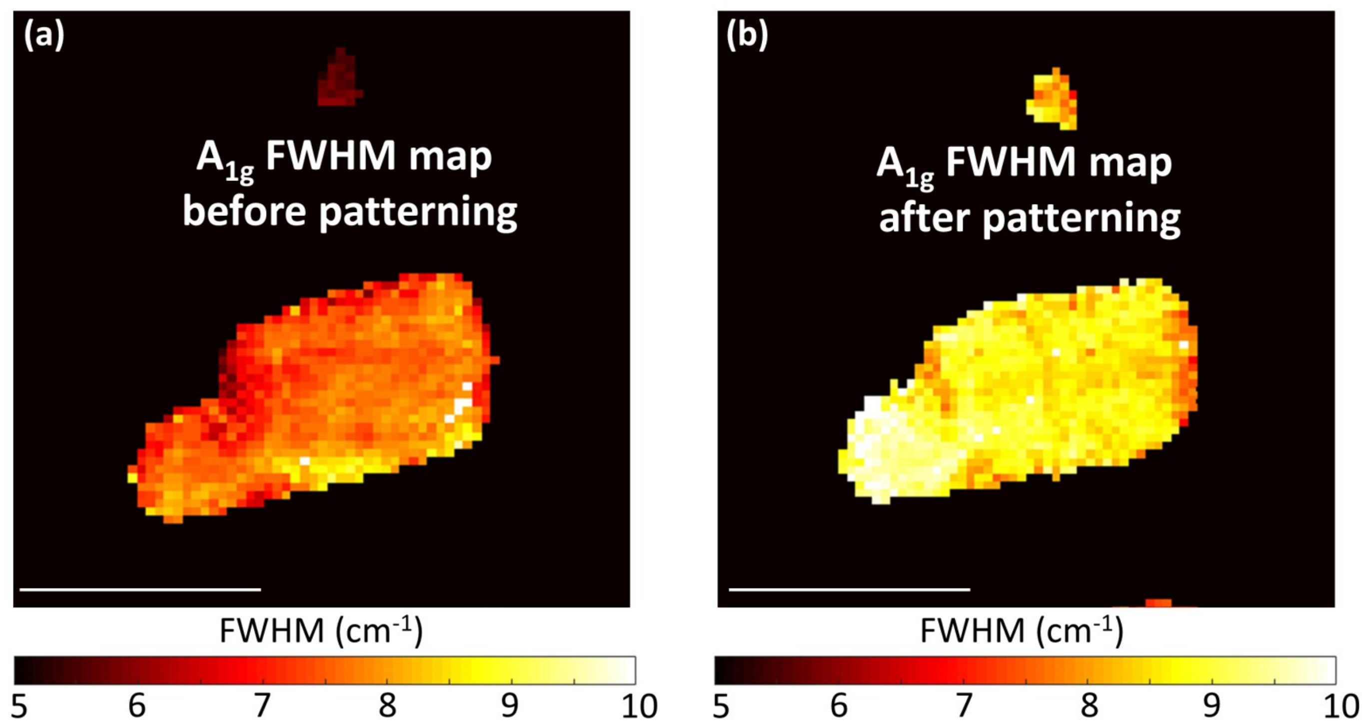

Fig.S6. A_{1g} FWHM Raman maps: (a) before PFEBIE. (b) after PFEBIE. An increase in FWHM is noticed. Scale bars are 2 µm.

Please do not adjust margins

Please do not adjust margins

Raman spectroscopy also gives information about the chemical composition. For that reason it is necessary to study Raman intensity maps before and after the patterning. Fig. S7 shows the Intensity maps of E^1_{2g} and A_{1g} peaks before and after PFEBIE. Fig. S4a and S4b correspond with the E^1_{2g} and A_{1g} maps before PFEBIE respectively. Fig. S4c and S4d correspond with the same Raman features after PFEBIE where the 250 nm narrowing is clearly observed. Both peaks were present after the patterning, indicating that the chemical composition has not been altered.

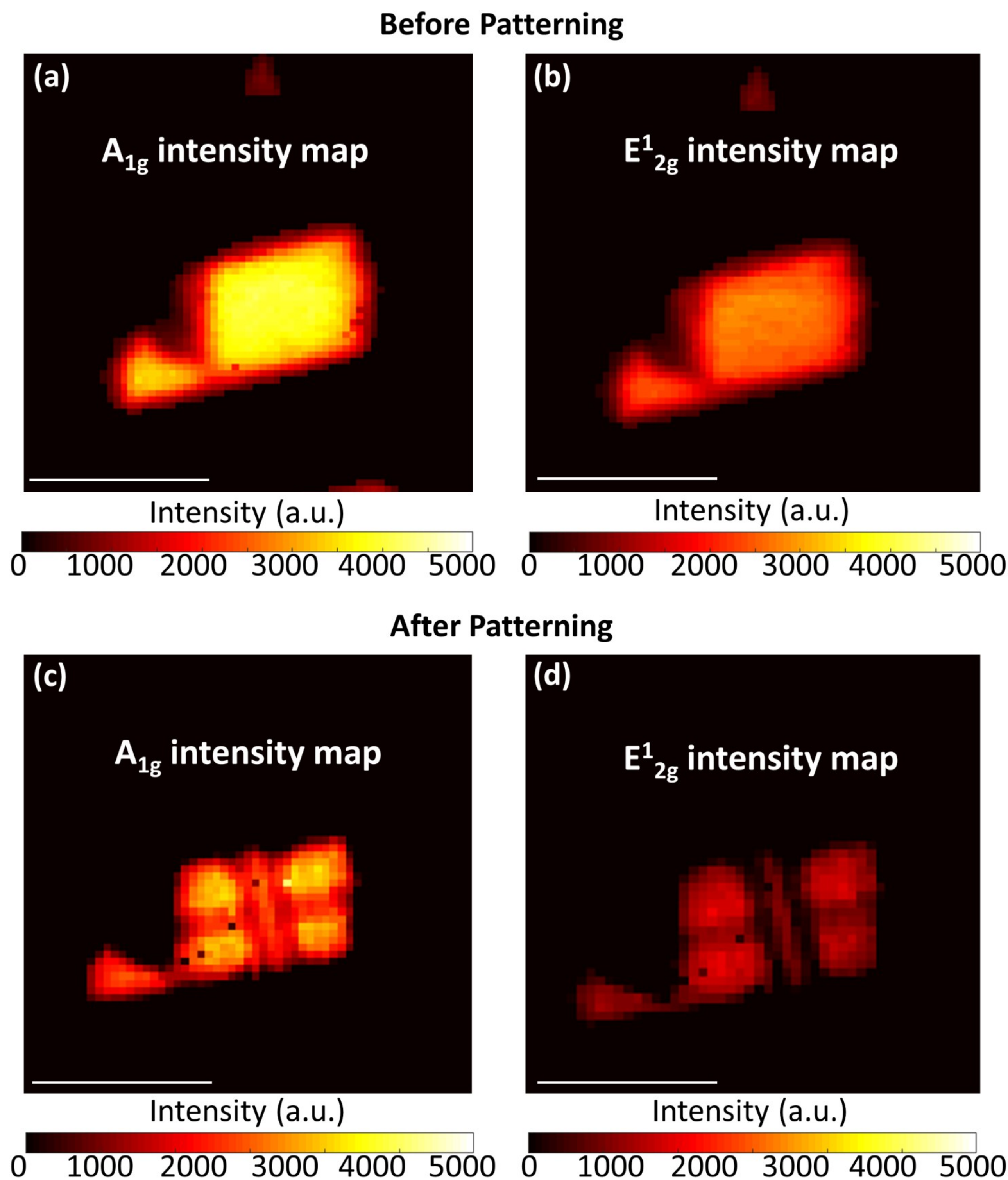

Fig.S7 (a) A_{1g} intensity map before PFEBIE. (b) E^1_{2g} intensity map before PFEBIE. (c) A_{1g} intensity map after PFEBIE. (d) E^1_{2g} intensity map after PFEBIE. Intensity maps after PFEBIE show the 250 nm narrowing. Scale bars are 2 µm.

This journal is © The Royal Society of Chemistry 20xx

Please do not adjust margins

Please do not adjust margins

Notes and references

1. A. Ortiz-Conde, F. J. Garcίa Sánchez, J. J. Liou, A. Cerdeira, M. Estrada and Y. Yue, *Microelectronics Reliability*, 2002, **42**, 583-596.
2. M. G. Stanford, P. R. Pudasaini, A. Belianinov, N. Cross, J. H. Noh, M. R. Koehler, D. G. Mandrus, G. Duscher, A. J. Rondinone, I. N. Ivanov, T. Z. Ward and P. D. Rack, 2016, **6**, 27276.
3. M. G. Stanford, P. R. Pudasaini, E. T. Gallmeier, N. Cross, L. Liang, A. Oyedele, G. Duscher, M. Mahjouri-Samani, K. Wang, K. Xiao, D. B. Geohegan, A. Belianinov, B. G. Sumpter and P. D. Rack, *Advanced Functional Materials*, 2017, **27**, 1702829.
4. E. S. a. A. V. K. Mahdi Ghorbani-Asl and Silvan Kretschmer and Douglas, *2D Materials*, 2017, **4**, 025078.
5. W. M. Parkin, A. Balan, L. Liang, P. M. Das, M. Lamparski, C. H. Naylor, J. A. Rodríguez-Manzo, A. T. C. Johnson, V. Meunier and M. Drndić, *ACS Nano*, 2016, **10**, 4134-4142.

Please do not adjust margins